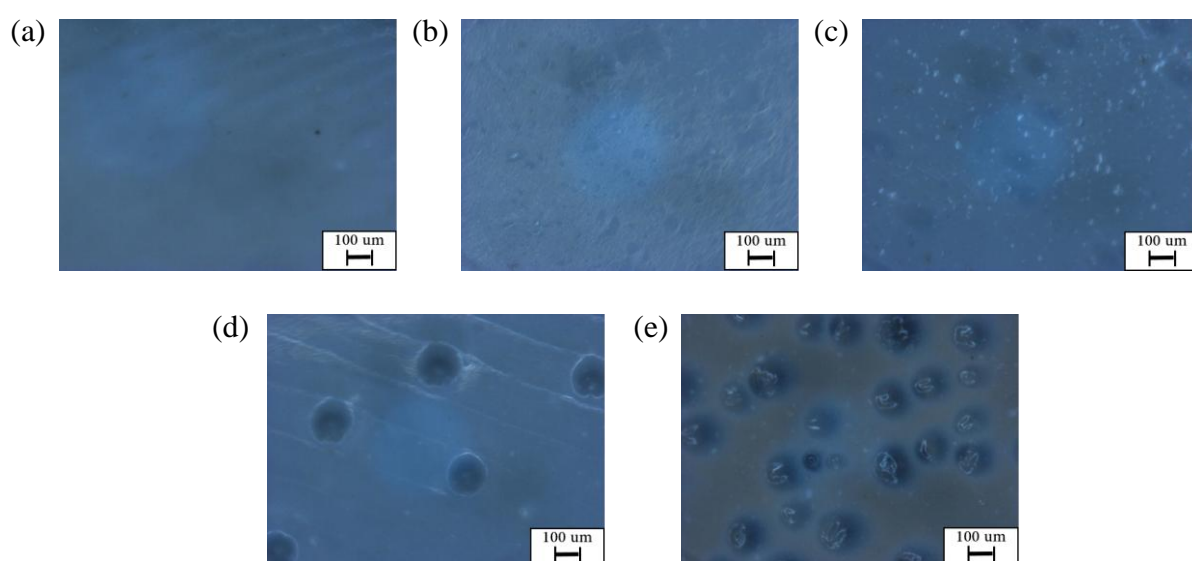


## Supporting Information

### 3D printing of Polyvinylidene Fluoride Based Piezoelectric sensors for Non-Invasive Continuous Blood Pressure Monitoring

*Arijit Mandal, Alban Morali, Maksim Skorobogatiy, and Sampada Bodkhe \**

#### S1. Microscopic images of PVDF nanocomposite films printed under various conditions



**Figure S1:** Microscopic images of PVDF nanocomposite films printed under various conditions: a) at ambient bed temperature, b) with a bed temperature of 40°C, c) 60°C, d) 80°C, and e) 100°C. (Printing speed: 20 mm.s<sup>-1</sup> nozzle diameter:0.25 mm, printing pressure:140 kPa, surface: air-side)

Figure 2 displays microscopic images of the films printed at various bed temperatures. Figures 2a, 2b, and 2c show no pores in the PVDF nanocomposite films subjected to ambient, 40°C, and 60°C bed temperatures. Conversely, Figures 2d and 2e illustrate the presence of pores when the films are subjected to bed temperatures of 80°C and 100°C. This pore formation is likely due to a faster evaporation rate.<sup>[1]</sup> These pores create challenges for the electrical poling process, as they serve as weak points where the electric field gets concentrated and causes dielectric breakdown at low electric fields, i.e., less than 10 MV m<sup>-1</sup>.<sup>[2]</sup>

## S2. Sensor attachment and hand support for wrist hyperextension and avoid movements

Sensor with  
tegaderm tape

Hand Support

Wrist Strap for  
securing the  
sensor

Collection BP  
waveform  
using sensor

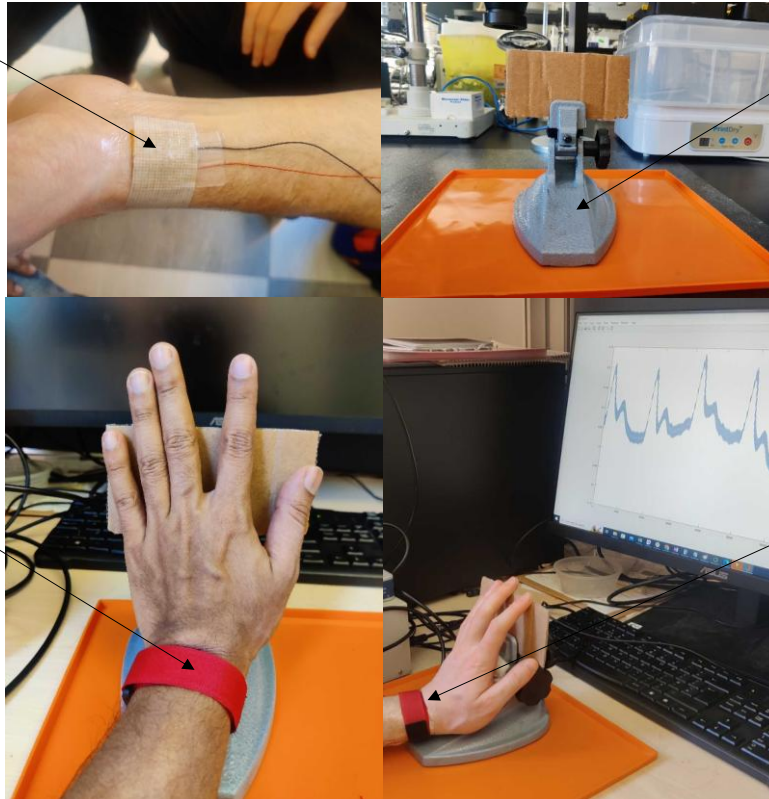


**Figure S2:** Hand support for taking (pulse pressure wave) PPW measurement from sensors

## S3. Determination of radial artery location using ultrasonic probe

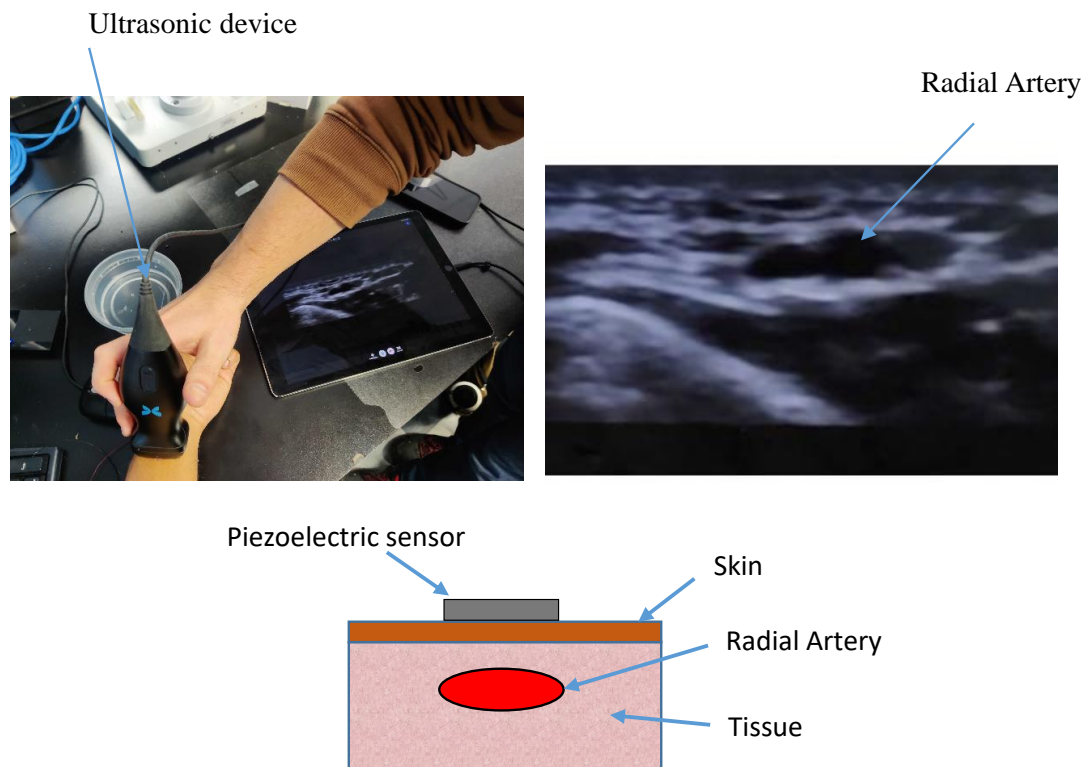
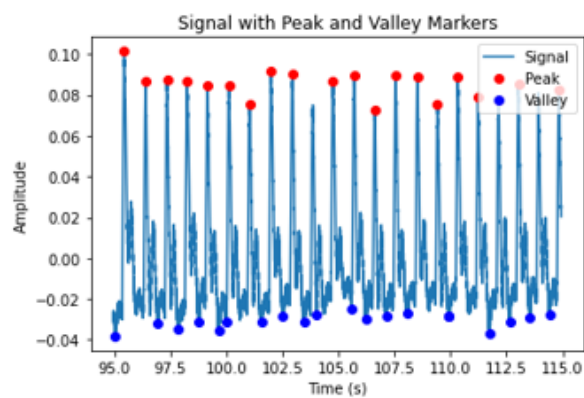


**Figure S3:** Ultrasonic view and schematic of radial artery

#### S4. Calibration process



Time(s)=95-114

Time (s)	Top Peaks (V)	Bottom Peaks (V)	Peak to Peak amplitudes(V)
95	0.1014	-0.0382	0.1396
96	0.0869	-0.0319	0.1188
97	0.0872	-0.0346	0.1217
98	0.0870	-0.0312	0.1182
99	0.0843	-0.0352	0.1195
100	0.0847	-0.0310	0.1157
101	0.0755	-0.0314	0.1069
102	0.0915	-0.0283	0.1197
103	0.0902	-0.0314	0.1216
104	0.0865	-0.0276	0.1141
105	0.0894	-0.0246	0.1140
106	0.0729	-0.0295	0.1024
107	0.0898	-0.0285	0.1184
108	0.0891	-0.0269	0.1161
109	0.0754	-0.0280	0.1034
110	0.0891	-0.0286	0.1177
111	0.0790	-0.0367	0.1157
112	0.0772	-0.0311	0.1084
113	0.0853	-0.0290	0.1142
114	0.0822	-0.0277	0.1099
Average	0.0852	-0.0306	0.1158

SBP=104  
DBP=65  
Heart Rate=55

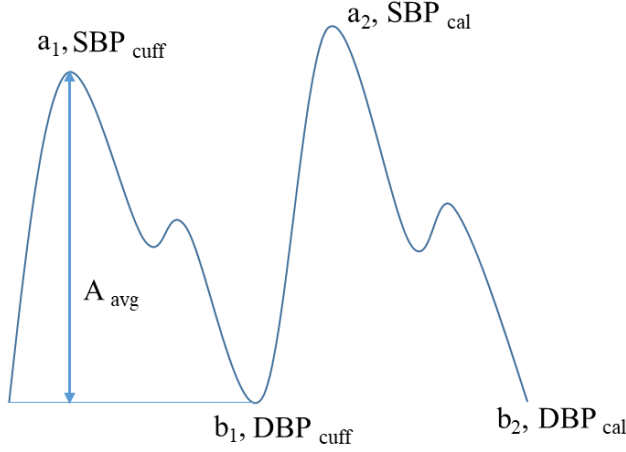


**Figure S4:** Calibration process of sensors with standard BP device (UA-767FAM)

First, the peak-to-peak amplitudes are calculated from the sensor data for the same time period as taken by the cuff to measure the blood pressure. As the cuff-based BP device give values over a period of time, we take out the average of peak to peak values of BP waveform from the sensor data and then use it for calibration as follows:

$$\text{Calibration ratio} = (\text{SBP}_{\text{cuff}} - \text{DBP}_{\text{cuff}}) / A_{\text{avg}}$$

$$\text{SBP}_{\text{cal}} = \text{SBP}_{\text{cuff}} + \text{Calibration ratio} * (a_2 - a_1)$$

$$\text{DBP}_{\text{cal}} = \text{DBP}_{\text{cuff}} + \text{Calibration ratio} * (b_2 - b_1)$$

where,

$\text{SBP}_{\text{cuff}}$  = Systolic BP measured by the cuff based device (Life Source UA-767FAM)

$\text{DBP}_{\text{cuff}}$  = Diastolic BP measured by the cuff based device

$A_{\text{avg}}$  = Average amplitude (in Volts) calculated from the sensor data for the time span taken by the cuff device to measure the BP

$\text{SBP}_{\text{cal}}$  = SBP calculated from sensor data after calibration

$\text{DBP}_{\text{cal}}$  = DBP calculated from sensor data after calibration

$a_1$  = Average of the peak voltage (in Volts) calculated from the sensor data for the time span taken by the cuff device to measure the BP

$a_2$  = Peak voltage for the next subsequent measurement after the calibration process

$b_1$  = Average of the valley voltage calculated from the sensor data for the time span taken by the cuff device to measure the BP

$b_2$  = Valley voltage for the next subsequent measurement after the calibration process

Then the calculated values from sensor after calibration are compared with cuff-based BP device for subsequent data collection.

### S5. Amplifier information

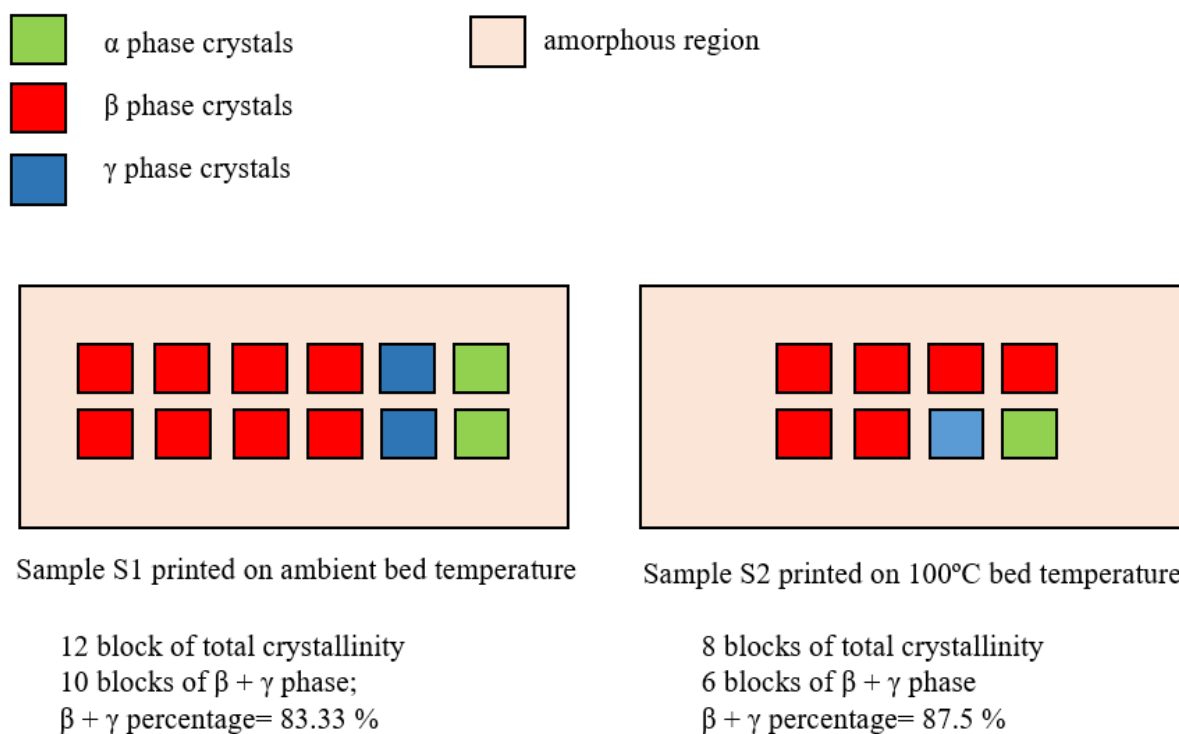


**Figure S5:** Piezo film lab amplifier

Piezo Film Lab amplifier (TE connectivity) was used to take measurement from the sensor using following settings:

- Mode: Voltage Mode
- Input Impedance: 1G (50 PF)
- Input Attenuator switch: 0 dB
- Low frequency Selector: 0.1 Hz
- High frequency Selector: 10 Hz

### S6. Schematic illustrating the crystalline composition of samples post-3D printing on a heated bed



Even though the  $\beta + \gamma$  percentage is high for sample S2 (87.5 %), the amount of  $\beta + \gamma$  phase is more in sample S1 as the total crystallinity is more

**Figure S6:** Schematic illustrating the crystalline composition of samples post-3D printing on a heated bed

## S7. Poling Process and its Influence on Piezoelectric Response Enhancement and Phase Transition in 3D Printed Materials

Poling is a fundamental step in enhancing the piezoelectric properties of PVDF composites. Primarily, the poling process facilitates the alignment of the  $\beta$ -phase chains, thereby amplifying the piezoelectric effect.<sup>[3]</sup> Based on recent investigations in our research group, we have discerned that the poling process can induce a conversion of the  $\gamma$ -phase into the  $\beta$ -phase.<sup>[4]</sup> This transformation not only augments the  $\beta$ -phase content by 40% within the crystal lattice but also results in a piezoelectric coefficient  $4.6 \pm 2$  pC/N.

- [1] D. Chen, T. Sharma, and J. X. J. Zhang, "Mesoporous surface control of PVDF thin films for enhanced piezoelectric energy generation," *Sensors and Actuators A: Physical*, vol. 216, pp. 196-201, 2014.
- [2] B. Zazoum, "Evaluation and Optimization of Dielectric Properties of PVDF/BaTiO<sub>3</sub> Nanocomposites Film for Energy Storage and Sensors," *ECS Journal of Solid State Science and Technology*, vol. 9, no. 11, 2020.

- [3] R. Tao, J. Shi, M. Rafiee, A. Akbarzadeh, and D. Therriault, "Fused filament fabrication of PVDF films for piezoelectric sensing and energy harvesting applications," *Materials Advances*, vol. 3, no. 12, pp. 4851-4860, 2022.
- [4] Alban Morali, Arijit Mandal, Maksim Skorobogaity, Sampada Bodkhe, "Unleashing the piezoelectric potential of PVDF: a study on phase transformation from gamma ( $\gamma$ ) to beta ( $\beta$ ) phase through thermal contact poling," *RSC Advances* (*submitted*), 2023.